

Metallurgical Stability and the Fracture Behavior of Ferritic Stainless Steels

C.H. Chun and D.H. Polonis

The influence of aluminum on the thermal stability of ferritic stainless steels has been investigated using two commercial alloys—Armco Type 18SR and AISI 430. Two reaction stages have been detected in these alloys during aging at 475 °C; each stage is accompanied by changes in the hardness, yield strength, strain-hardening exponent, and elongation to fracture. The initial stage is attributed to the precipitation of carbide and nitride particles and the second stage to the precipitation of the chromium-rich α′ phase. The 430 alloy exhibits more pronounced changes than 18SR during the first stage due to the higher concentration of interstitials retained in solution after quenching. The effects of the second-stage aging reaction are detected after shorter aging times in the 18SR alloy and are more pronounced than in the 430 alloy, consistent with the influence of aluminum on the coherency strains associated with α′ precipitation. The fracture mechanism in both alloys changes from ductile dimples in the solution-treated and quenched condition to a mix of ductile dimples, intergranular fracture, and transgranular cleavage with increased aging times. Longitudinal cracking at the grain boundaries precedes failure of the aged alloys in tension; it is attributed to the combined effects of void initiation at fine grain boundary precipitates, α′ embrittlement that limits localized plasticity, and the transverse stress components resulting from triaxiality after the onset of necking.

1. Introduction

FERRITIC stainless steels containing more than about 13 wt.% chromium are subject to a form of embrittlement, known as 475 °C embrittlement, when exposed to temperatures above 400 to 550 °C.[1-6] This behavior limits the use of such steels for elevated temperature applications, particularly because the reaction can occur during heating and cooling cycles through this temperature range. The embrittlement mechanism has been identified with the precipitation of a chromium-rich body-centered cubic phase designated α′, which forms due to a miscibility gap in the iron-chromium system.[1,2,4,6,7,8] The presence of the α′ phase causes a marked increase in hardness and strength, but is accompanied by dramatic decreases in the ductility and toughness,[1-6] plus changes in electrical resistivity, magnetic properties, and corrosion resistance. Most of the previous studies of 475 °C embrittlement have concentrated on the accompanying changes in mechanical properties including hardness, tensile, and impact behavior.

The ductility of ferritic iron-chromium alloys is also affected by the presence of interstitials, thereby complicating attempts to define the specific contribution of the α′ phase to the embrittlement and loss of toughness. Binder and Spendelow[9] demonstrated that the carbon and nitrogen limits required to ensure good room-temperature toughness must be reduced when the chromium content is increased over the range 12 to 40%, *e.g.*, from 550 ppm at 18% Cr to 350 ppm at 30% Cr. Above these limits, the alloys tended to be brittle at room temperature, but in alloys with a low (C + N) level the ductile-to-brittle transition temperature (DBTT) values are sensitive to post-annealing cooling rates and can be altered significantly by heat treatment. Plumtree and Gullberg[10] showed that rapid cooling rates enhance the toughness of iron-chromium alloys with low (C + N) contents. They showed that the embrittlement associated with slow cooling rates was related to carbide and nitride precipitation and identified a grain boundary phase as Cr_2N.

Relatively little information has been reported relevant to the micromechanisms of the fracture process in ferritic iron-chromium alloys, especially with respect to the initiation of fracture and the relative roles assumed by ductile flow, cleavage, and intergranular cracking in the overall failure process. The influence of alloy additions on the susceptibility of iron-chromium alloys to embrittlement is of continuing interest. Conflicting results have been reported about the effectiveness of aluminum additions in slowing the 475 °C embrittlement reaction and reducing the detrimental effects of interstitials.[3,5,6,11,12] The present work examines the relationships between the mechanical strength and fracture mechanisms, especially with respect to the role assumed by the embrittlement reaction and the difference in fracture behavior of two similar iron-chromium alloys, one of which contains 2% Al.

2. Experimental Procedures

Two commercial alloys—Armco Type 18SR and AISI 430—were chosen for this investigation to determine the influence of aluminum on the process of embrittlement and fracture. Table 1 contains the compositional analyses of these alloys. Specimens for microhardness and tensile tests were cut from annealed panels of both alloys. Sheet tensile specimens were machined with a gauge length of 25.4 mm, a width of 20.6 mm, and sheet thickness of 0.72 mm, with the rolling direction parallel to the specimen axis. The specimens were hand polished with 320- and 600-grit grinding papers prior to testing. The tensile specimens were solution treated at 885 °C in flowing, purified argon prior to quenching; aging was carried out in molten salt baths controlled to ±1 °C for periods up to 1000 hr at temperatures ranging from 400 to 550 °C. Room-temperature ten-

C.H. Chun and **D.H. Polonis**, Department of Materials Science and Engineering, University of Washington, Seattle, Washington.

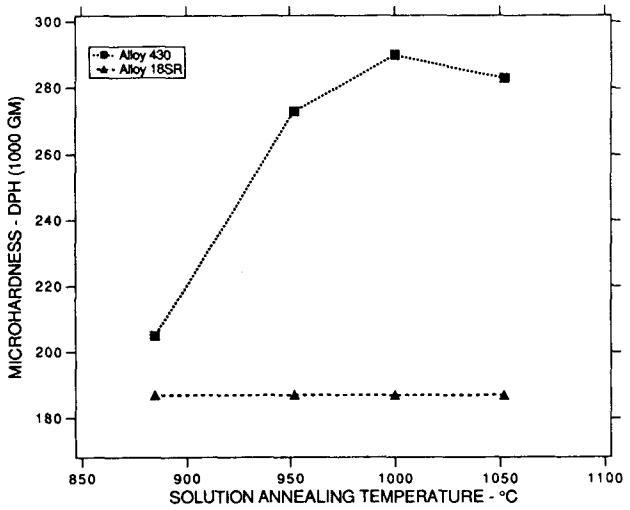

Fig. 1 Room-temperature hardness as a function of solution temperature for alloys 18SR and 430.

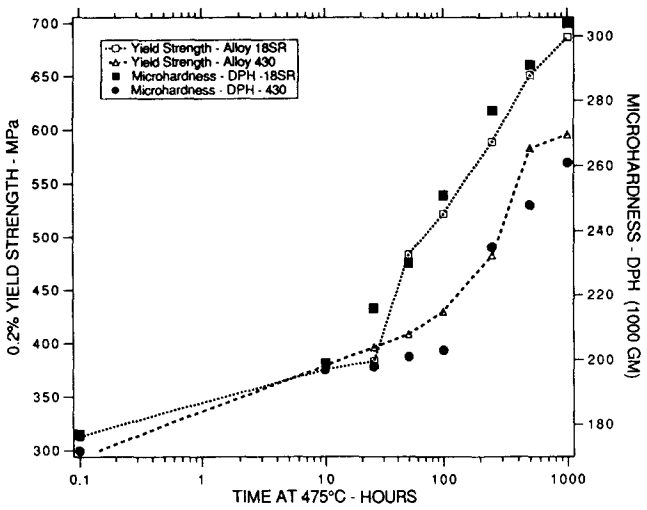

Fig. 2 Influence of aging time at 475 °C on the yield strength and hardness of the 18SR and 430 alloys.

Table 1 Chemical Composition of Alloys

	Composition																	
	C		Mn		P		S		Si		Cr		Ti		Al		Ni	
Alloy	wt.%	at.%	wt.%	at.%	wt.%	at.%	wt.%	at.%	wt.%	at.%	wt.%	at.%	wt.%	at.%	wt.%	at.%	wt.%	at.%
Alloy 18SR	0.033	0.146	0.16	0.155	0.02	0.034	0.015	0.026	0.6	1.14	17.28	17.72	0.39	1.12	1.76	3.48	0.3	0.27
Alloy 430	0.056	0.255	0.34	0.339	0.014	0.025	0.01	0.017	0.36	0.7	16.87	17.76	...	...	...	...	...	...

sile tests were conducted to fracture using an Instron Universal testing machine in accordance with ASTM A-370 and E-8 specifications. A crosshead speed of 0.05 cm/min was used, which corresponds to an approximate strain rate of 3.3×10^{-4} sec^{-1}. Microhardness measurements employed a standard Vickers diamond pyramid hardness tester with a 100-g load. The reported hardness values were based on at least ten separate measurements.

Specimens for optical metallographic examination were prepared by mechanical polishing, followed by etching in a mixture of glacial acetic acid, concentrated nitric acid, and concentrated hydrochloric acid (1:1:3 parts by volume). Scanning electron micrograph (SEM) techniques were used to examine fracture surfaces.

3. Experimental Results

3.1 *Solution and Aging Temperature Effects*

Samples of both alloys were solution treated at several temperatures over the range 885 to 1050 °C, followed by water quenching. The results are plotted in Fig. 1, which shows a marked increase in the room-temperature hardness with increasing solution temperature for the 430 alloy, but no significant change for the 18SR alloy. Figure 2 shows that the microhardness of both alloys increased slightly from the solution treated value during the initial 10 hr of aging at 475 °C. The hardness of the 18SR alloy continued to increase with increasing aging time at 475 °C; however, the hardness of the 430 alloy remained essentially unchanged over the aging period of 10 to 100 hr. Figure 2 also shows that continued aging of the 430 alloy beyond 100 hr at 475 °C resulted in a second-stage reaction involving significant increases in the hardness and yield strength. Both alloys exhibited hardness increases at higher and lower aging temperatures (400 and 550 °C), but the magnitudes of the changes were much more gradual than at 475 °C, as shown in Fig. 3(a) and (b).

3.2 *Tensile Yield Strength*

Room-temperature tensile tests were performed on the 430 and 18SR alloys after solution annealing at 885 °C, followed by quenching and then aging at temperatures in the range 400 to 550 °C for times up to 1000 hr. Figure 4 shows that the change in the 0.2% yield strength with aging time at 475 °C parallels the two-stage increase in hardness and is accompanied by corresponding decreases in elongation, as shown in Fig. 4. The yield strength and the hardness increased more rapidly in the 18SR alloy; also the total aging time prior to the start of the second stage hardness increase was only 10 hr for the 18SR alloy compared to 80 hr for the 430 alloy. The 0.2% yield strength of the 18SR alloy increased to 687 MPa after 1000 hr at 475 °C, compared to 596 MPa for the 430 alloy. The strain-hardening exponents, determined from plots of log stress versus log strain, decreased with increasing aging time at 475 °C, as shown in Fig. 5. Tensile test results for specimens aged at 400 and 550 °C are shown in Fig. 6(a) and (b). The 18SR data reflect

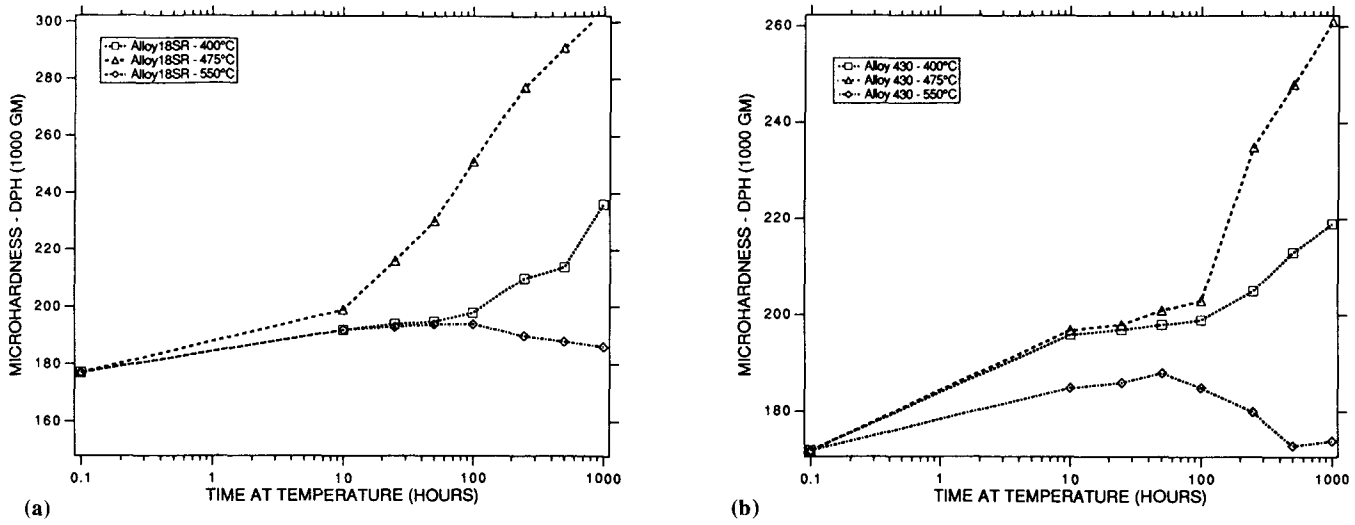

Fig. 3 Effects of aging temperature on the hardness versus aging time for **(a)** alloy 18SR and **(b)** alloy 430.

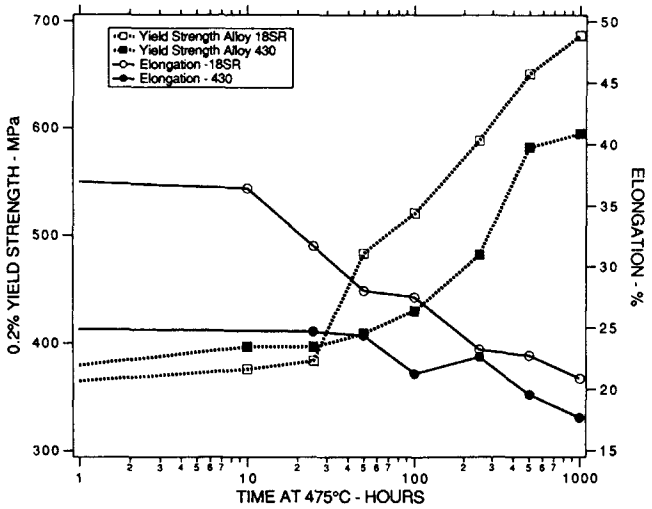

Fig. 4 Influence of aging time at 475 °C on the 0.2% yield strength and the elongation to fracture of the 18SR and 430 alloys.

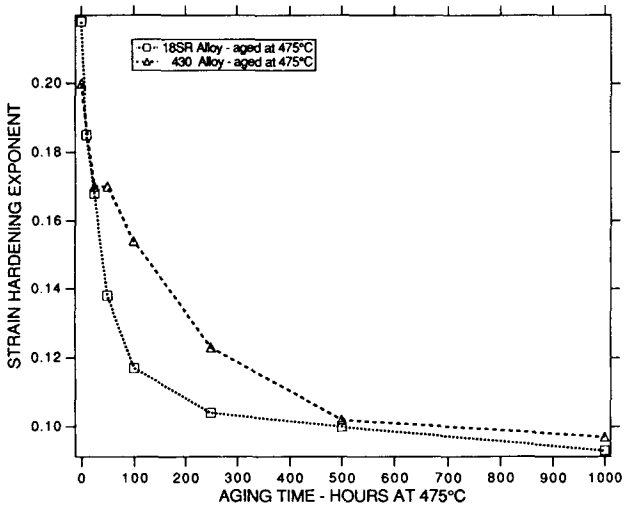

Fig. 5 Effects of aging time at 475 °C on the strain-hardening exponent of the 18SR and 430 alloys.

two-stage aging behavior at 400 °C, whereas the 430 results suggest that the second stage is suppressed. The tensile results after aging for periods up to 1000 hr at 550 °C showed no consistent increase or decrease in the yield strength for both alloys.

3.3 *Tensile Elongation*

The effects of aging time at 475 °C on the tensile elongation to fracture of the 18SR and 430 alloys are included with the tensile test results in Fig. 4. The elongation of the 18SR alloy decreased rapidly from 39% in the quenched condition to 28% after 50 hr at 475 °C, following which a gradual decrease to approximately half of the quenched value occurred after aging 1000 hr. The 430 alloy showed no significant decrease in elongation during the initial 50 hr at 475 °C, following which a gradual decrease from 25 to 18% occurred after 1000 hr. Figures 6(a) and (b) show the 18SR alloy as having greater ductility in tension than the 430 alloy for all aging times at 475 °C. The elongation results for aging at 400, 475, and 550 °C are combined with the yield strength plots in Fig. 6(a) and (b). No significant changes in tensile elongation with increasing aging time were detected at 550 °C, but the trends at 400 °C were consistent with those for the yield strength, with a gradual decrease in elongation occurring in the 18SR alloy after 100 hr and no significant change in the 430 alloy.

3.4 *Metallographic Observations*

The microstructures of the 18SR and 430 ferritic steels exhibited average grain sizes of 15 to 17 μm; representative mi-

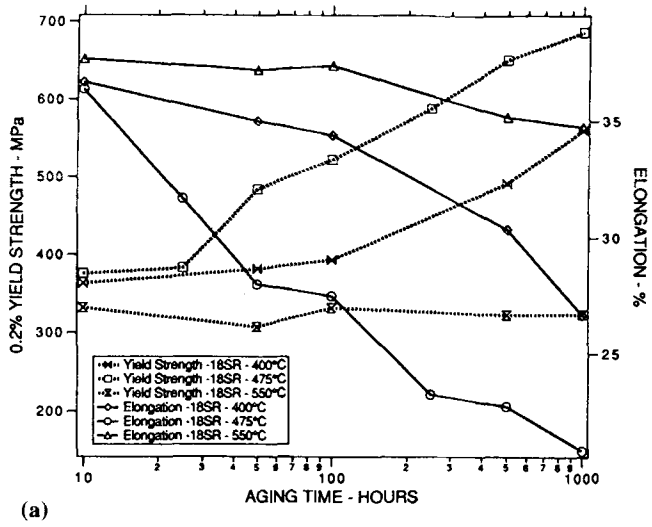

(a)

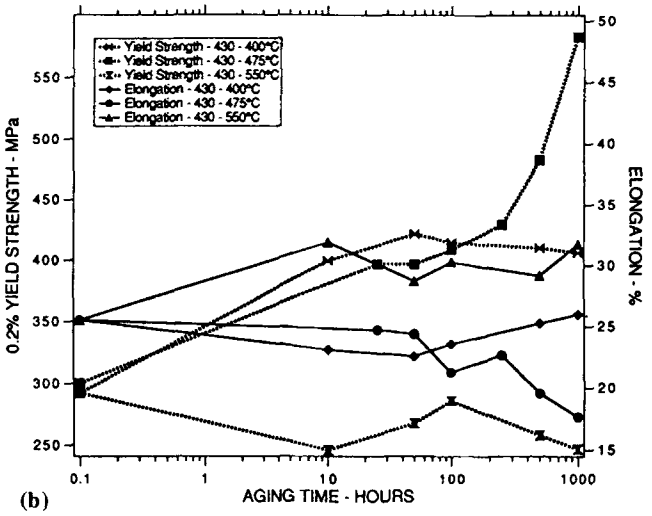

(b)

Fig. 6 Tensile test results showing the effects of aging temperature and aging time on the 0.2% yield stress and the elongation to fracture for the **(a)** 18SR and **(b)** 430 alloys.

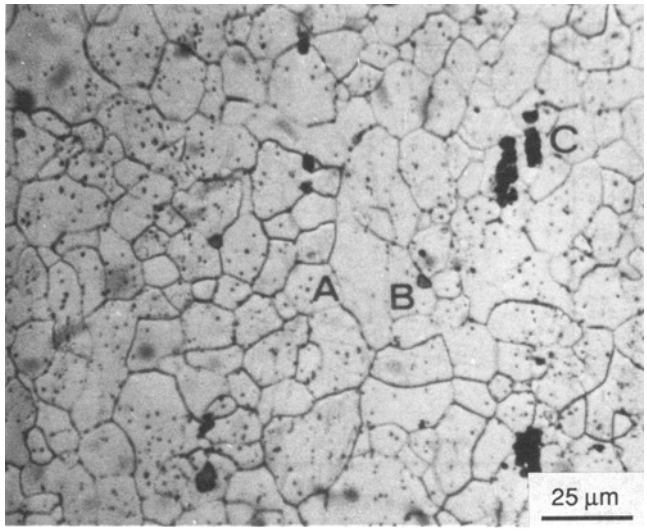

(a)

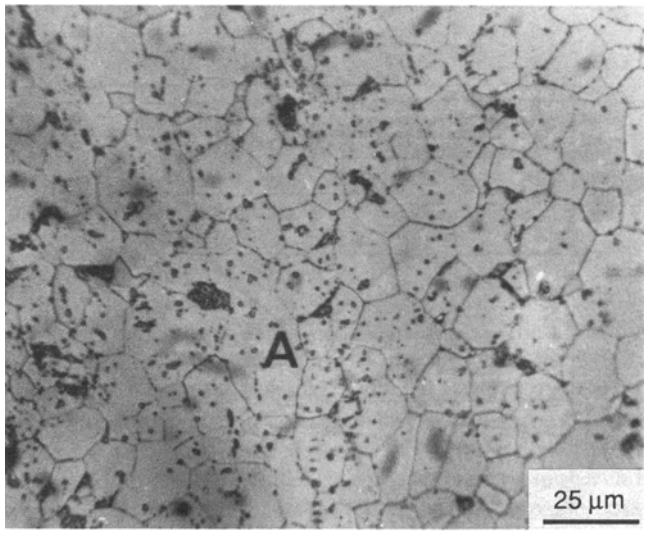

(b)

Fig. 7 Optical microstructures after aging 1000 hr at 475 °C. **(a)** 18SR alloy, showing fine carbides and nitrides dispersed randomly and at grain boundaries (A), plus "blocky" titanium carbides (B), some of which are clustered as at C. **(b)** 430 alloy, showing only fine, dispersed carbides and nitrides (A).

crographs are shown in Fig. 7(a) and (b) for both alloys in the quenched and aged condition. The 18SR alloy exhibited fine, dispersed carbide and nitride particles after quenching from 885 °C (A in Fig. 7a) and larger, blocky particles (B in Fig. 7a), some of which occur in clusters (*e.g.*, C in Fig. 7a). These particles were identified by EDAX as titanium rich. The 430 alloy exhibited a higher density of fine carbides and nitrides than the 18SR alloy, as shown in Fig. 7(b), due to slightly higher carbon content. However, the 430 alloy did not contain the larger titanium-rich particles.

The only microstructural change observed in the quenched alloys at optical magnifications, after aging for 1000 hr at 475 °C, was the precipitation of additional fine carbide and nitride particles during the initial stage of aging. Scanning electron microscopy was used to examine the effects of aging on the fracture modes in both alloys; the observations are summarized in Table 2. The SEM observations, as shown in Fig. 8 and 9, were correlated with fracture profile examinations using optical microscopy, the results of which are also summarized in Table 2. Where appropriate, the orientations of the specimen thickness direction (TD) and the tensile axis (TA) are indicated on the photomicrographs.

The SEM studies of fracture surfaces from the solution-treated and quenched 18SR and 430 alloys revealed predominantly ductile dimple fracture, as shown in Fig. 8(a) and (b); the dimples were generally larger and deeper in the 18SR alloy and exhibited more evidence of shear. The nucleation of dimples in both alloys was generally associated with the presence of fine second-phase particles similar to those identified as carbides or nitrides in the original solution-treated condition. After 1000 hr

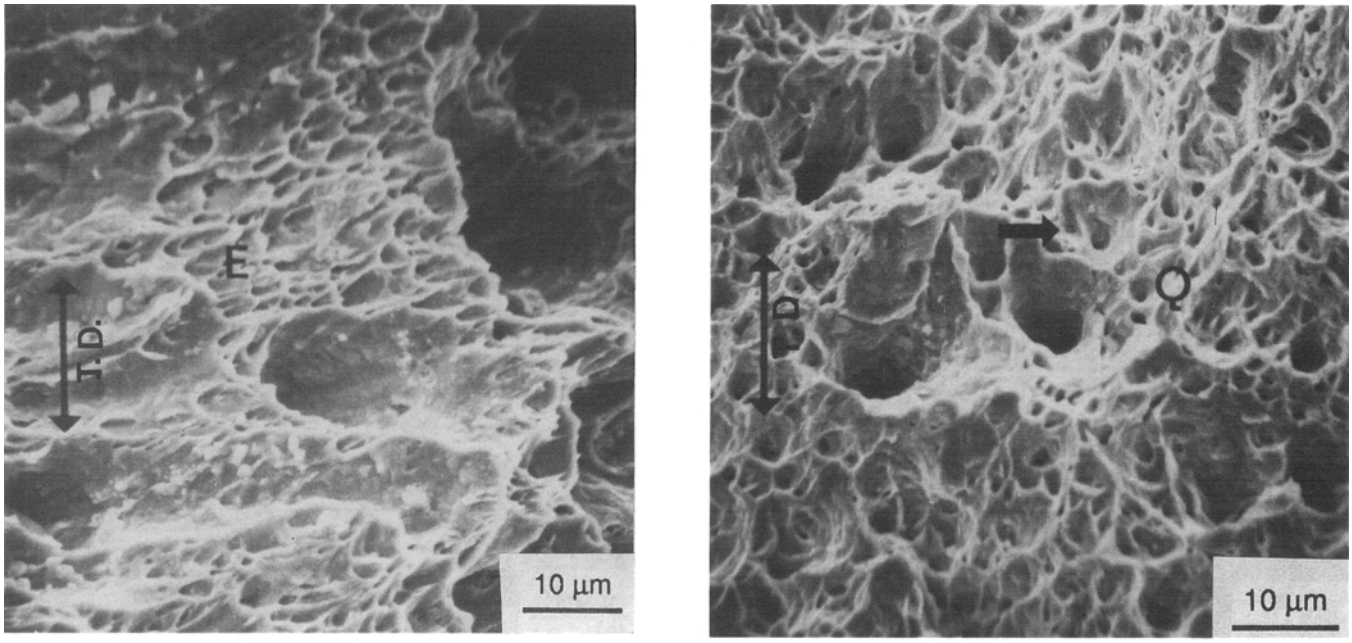

Fig. 8 SEM fractographs from the solution-treated and quenched alloys. **(a)** Type 18SR, showing large, deep dimples and elongated dimples (E). **(b)** Type 430, showing a predominance of fine, equiaxed dimple structures (Q).

Table 2 Summary of Effects of Aging on Fracture Behavior

Aging condition	Fracture surface profile		SEM fracture surface observations	
	18SR alloy	430 alloy	18SR alloy	430 alloy
Solution annealed	Microvoids at TiC particles	Microvoids, inclusions	Completely ductile dimple	Completely ductile dimple
Aged 50 hr at 475 °C	Microvoids, intergranular cracks	Microvoids	Completely ductile dimple	Completely ductile dimple
Aged 100 hr at 475 °C	No. of intergranular cracks increases and density of	Microvoids		
Aged 250 hr at 475 °C	microvoids gradually decreases with aging time.	Microvoids		
Aged 500 hr at 475 °C	All intergranular cracks are parallel to tensile axis	Microvoids + intergranular cracks		
Aged 1000 hr at 475 °C	Few microvoids, numerous intergranular cracks, mostly at mid-thickness in neck	Increase in No. of intergranular cracks	Mixed fracture modes: cleavage, intergranular, ductile dimple	Predominantly ductile dimple + few intergranular facets
Aged 1000 hr at 400 and 550 °C	Microvoids	Microvoids		

of aging at 475 °C, the 18SR alloy exhibited a mixed fracture mode consisting of ductile dimples, transgranular cleavage, and numerous secondary intergranular cracks parallel to the flat surface of the tensile specimen; these features are shown in Fig. 9(a), (b), and (c). The fracture surfaces of the 430 alloy showed microvoid coalescence to be the predominant fracture mode, even after 1000 hr of aging at 475 °C, with occasional evidence of intergranular facets and quasi-cleavage (*i.e.*, cleavage lacking a definite orientation relationship with that of the crystal), as shown in Fig. 10.

3.5 *Fracture Surface Profiles*

Fractured tensile specimens were sectioned throughout their mid-widths so that the plane of polish corresponded to a thickness plane normal to the sheet surfaces of the tensile specimens; the observations of the fracture profiles are summarized in Table 2 and examples of the micrographs are given in Fig. 11 to 14, respectively. The fracture profile of the 18SR alloy, after aging for 50 hr at 475 °C, revealed a ductile failure mode, with numerous voids initiated at second-phase particles identified by EDAX as titanium carbides or carbon nitrides (see Fig. 11a and b). Continued aging beyond 50 hr at 475 °C revealed an increasing tendency for intergranular crack development parallel to the tensile axis, as shown in Fig. 12(a) and (b), and a decrease in void density. The intergranular cracks were frequently associated with voids formed adjacent to coarse boundary precipitates, as shown in Fig. 11(b) and 12(b). These cracks occurred primarily near the mid-section of the tensile specimens, in agreement with the SEM fracture surface observations,

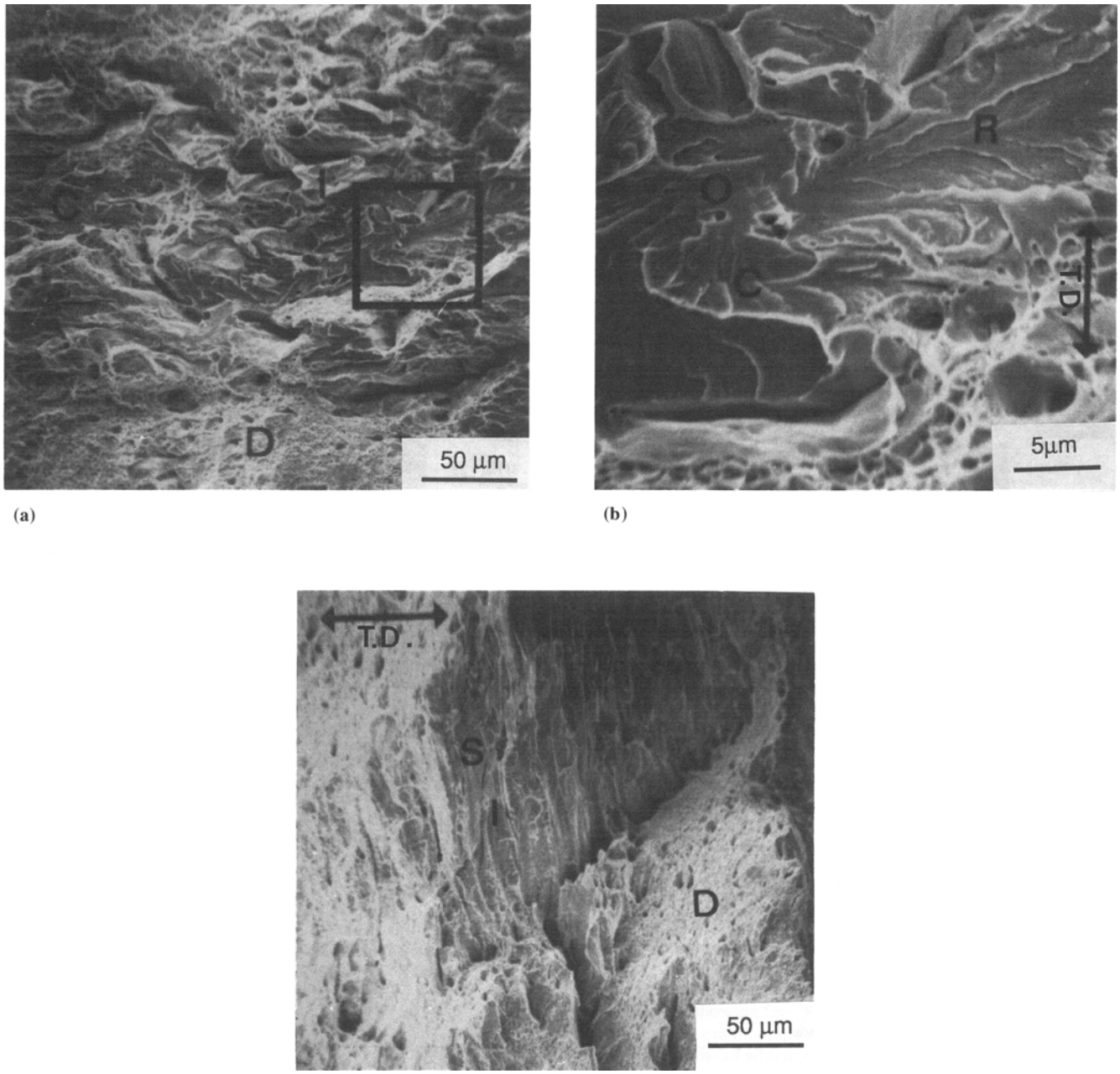

Fig. 9 SEM fractographs of type 18SR aged 1000 hr at 475 °C. **(a)** A mixture of ductile dimples (D), transgranular cleavage (C), and secondary intergranular cracks (I) parallel to the flat surface of the tensile specimen. **(b)** Higher magnification of the region outlined in **(a)**, showing cleavage steps (C), river patterns (R), and a likely cleavage initiation center (O). **(c)** Intergranular fracture viewed with specimen tilted 28° in the microscope, showing a mix of dimples (D) and smooth, curved facets (I) containing wavy slip lines (S) suggesting significant plasticity prior to fracture in regions adjacent to the grain boundary.

whereas dimples were confined primarily to the outer surface regions. The tendency for mixed modes of fracture to occur after aging was confirmed by examining the profiles of specimens sectioned to the mid-thickness, *i.e.*, observing a plane of polish parallel to the flat external surfaces of the tensile specimens, but at the mid-thickness. Figures 13(a) and (b) illustrate the mixed fracture modes exhibited by the 18SR alloy after aging 1000 hr at 475 °C; the failure process includes cleavage and intergranular fracture, combined with extensive plastic strain.

Fracture surface profile examination confirmed that the fracture process in the 430 alloy was induced primarily by voids in the solution-treated condition (Fig. 14) and after aging treatments of up to 500 hr at 475 °C (Fig. 15). The fracture profiles were much more irregular than those of the 18SR alloy due

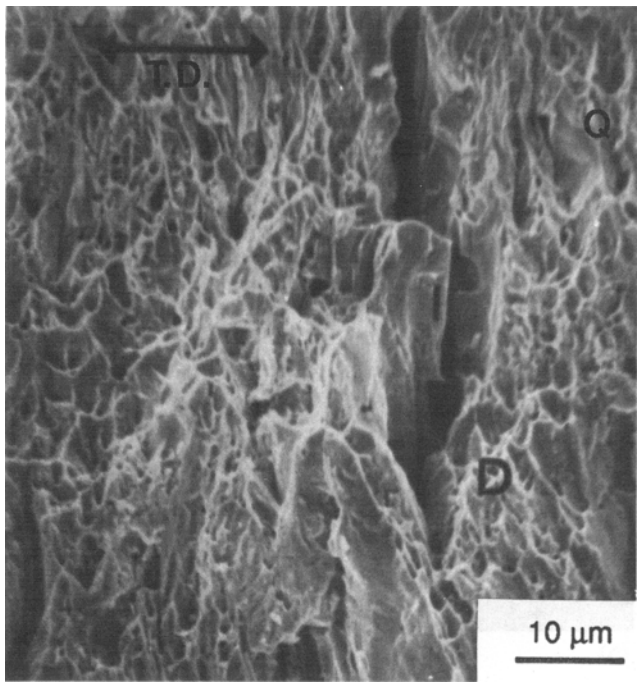

Fig. 10 SEM fractograph of type 430 aged 1000 hr at 475 °C, showing microvoids (D) with some evidence of intergranular cracking (I) and "quasi-cleavage" (Q).

to the high density of microvoids and the extensive plasticity adjacent to the fracture surface, as shown in Fig. 14 and 15. Intergranular cracking was observed in specimens of the 430 alloy aged for 500 hr at 475 °C (Fig. 15) and was more prominent after 1000 hr, as shown in Fig. 16. However, evidence of extensive plasticity and void development persisted.

4. Discussion

4.1 *Solution-Treated Condition and Initial Stage of Aging*

The influence of the aluminum and titanium contents in the 18SR alloy is apparent when comparing the properties with those of the 430 alloy. The increase in hardness of the 430 alloy after quenching from successively higher temperatures up to 1050 °C, as shown in Fig. 1, can be attributed to an increase in the dissolution of chromium carbides and nitrides for solution temperatures above 850 °C.[13] The relatively high hardness of the 430 alloy after solution treatment and quenching has been explained in terms of either the retention of clustered carbon and nitrogen atoms in supersaturated solution[14] or fine precipitation at dislocation sites.[15] Both processes are expected to increase the flow stress and decrease the ductility. Figure 1 shows that the hardness of the 18SR alloy, after quenching from temperatures ranging from 850 to 1050 °C, is relatively insensitive to the solution temperature; this is consistent with the ability of titanium and aluminum to form stable carbides and nitrides, respectively, thereby reducing the levels of carbon and nitrogen in solution.

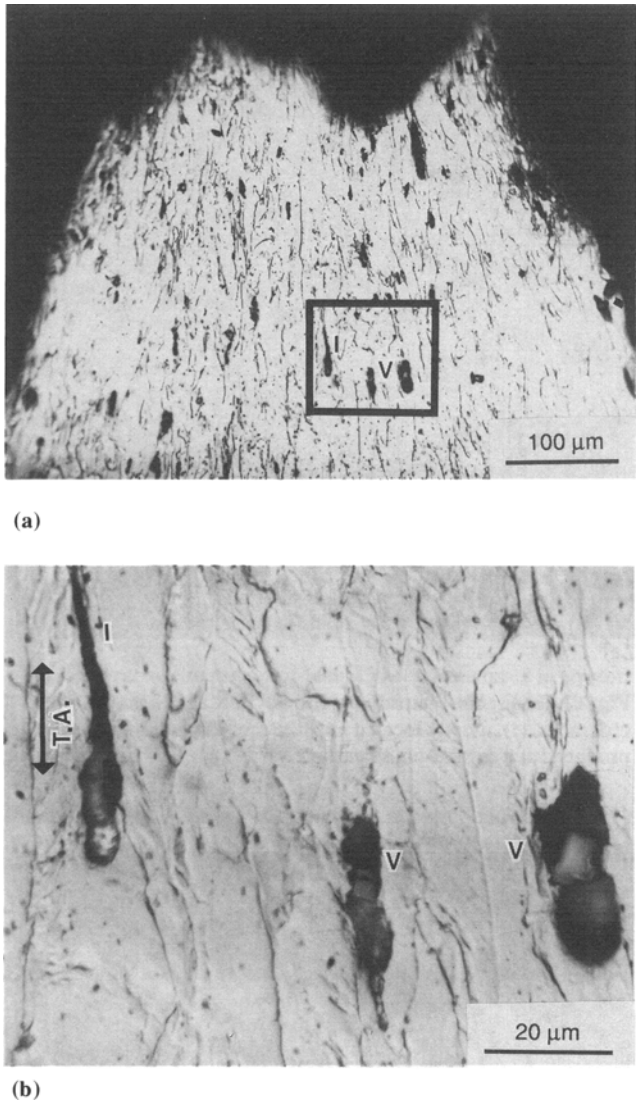

Fig. 11 Fracture profile of type 18SR aged 50 hr at 475 °C. **(a)** Early stages of longitudinal intergranular cracking (I) and void generation (V). **(b)** Enlarged view of the region outlined in **(a)**, indicating titanium carbonitride particles as the likely nucleating sites or voids (V).

It has been reported[16,17] that weight ratios of titanium to (C + N) of approximately 10 can combine with the majority of (C + N), although some interstitials are expected to remain in solution and will be precipitated during aging at lower temperatures. The influence of such precipitation is shown in Fig. 2 and 3(b), in which the hardness of the 430 alloy increases rapidly during the initial 10 hr of aging, followed by a hardness plateau prior to the continuous increase identified with the precipitation of the α' phase after approximately 100 hr. Similar aging behavior has been noted in several other commercial ferritic stainless steels containing 18 to 29% Cr.[18] The initial stage of aging in the 430 alloy is accompanied by the precipitation of carbides and nitrides and is consistent with the observations reported for other ferritic alloys.[10,19] The 18SR alloy exhibits a

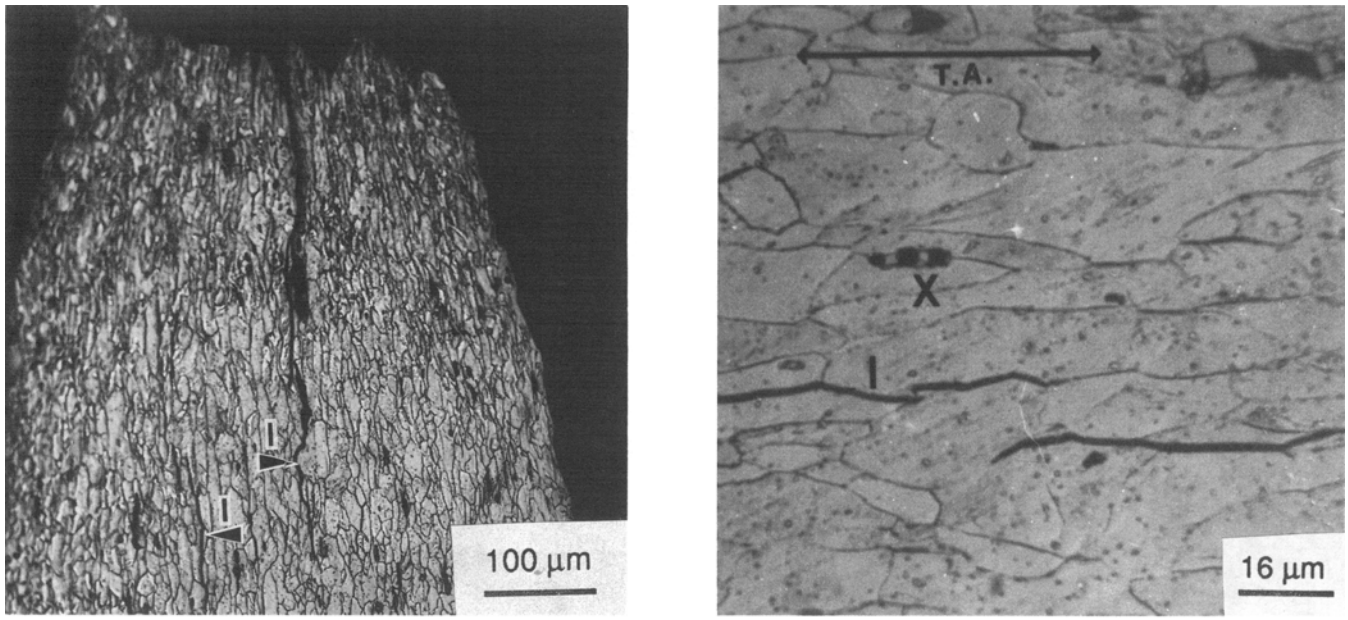

(a) (b)

Fig. 12 (a) Fracture surface profile of 18SR aged 1000 hr at 475 °C, showing relatively few voids, but well-defined intergranular microcracks, (I), mostly located near the mid-thickness of the tensile specimen. (b) Intergranular fracture parallel to the tensile axis and a void produced at a second-phase particle.

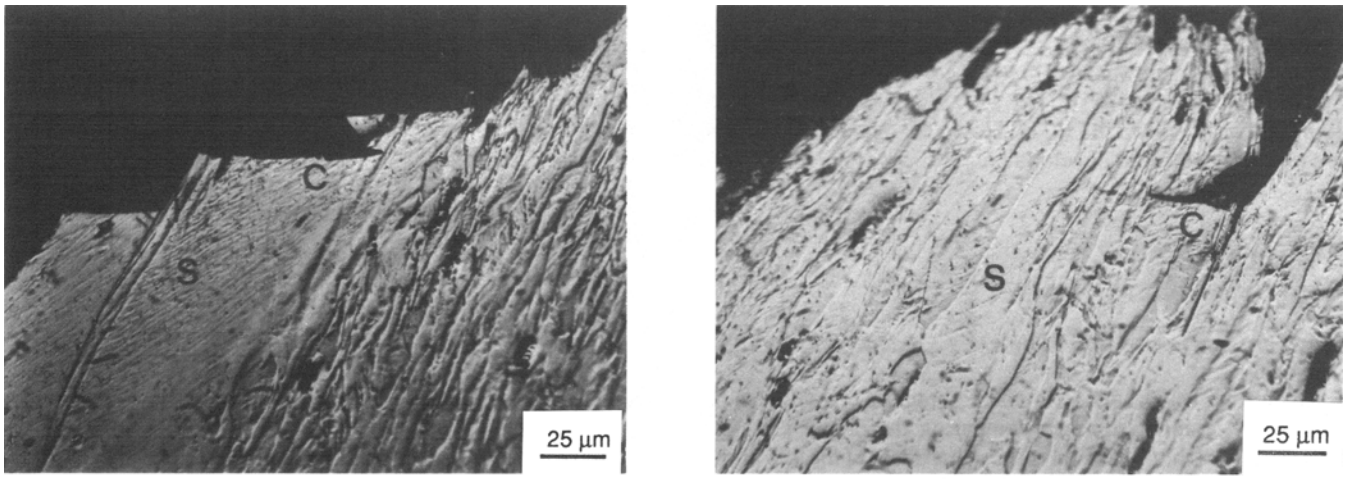

(a) (b)

Fig. 13 Fracture surface profiles showing mixed fracture modes characteristic of the 18SR alloy subjected to tension after aging 1000 hr at 475 °C. (a) Cleavage and (b) mixed cleavage and ductile flow.

less well-defined initial stage of precipitation, because the presence of aluminum and titanium in this alloy promotes the formation of stable nitrides and carbides at the solution temperature. The hardness and yield strength of the 18SR alloy increase in a more continuous manner with aging time, as shown in Fig. 2 and 3(a).

The fracture surfaces of the 18SR and 430 alloys exhibited ductile dimples due to microvoid growth in the solution-treated and quenched condition. The larger and deeper dimples observed on the fracture surfaces of the 18SR alloy are consistent with the important role of the coarse titanium carbide particles in initiating the fracture process. The higher ductility of the 18SR alloy in the quenched condition is consistent with the elongated and sheared appearance of the dimples in Fig. 8(a).[20] The higher volume fraction of carbide particles in the 430 alloy is expected to increase the number of localized plastic strain centers,[21] which in turn accounts for the finer dimple structure observed on the fracture surfaces of this alloy. The

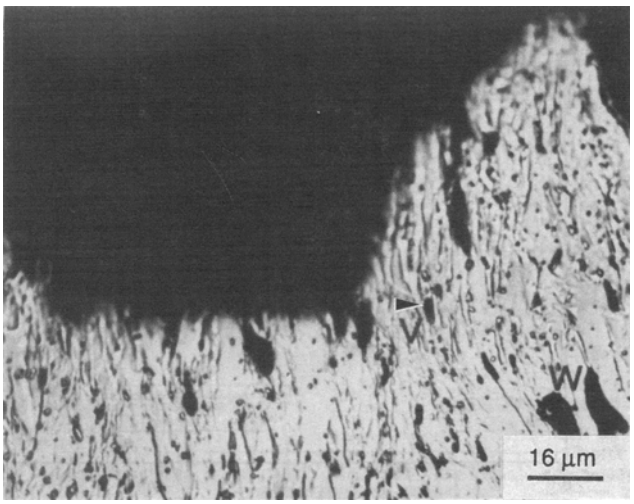

Fig. 14 Fracture surface profile of 430 alloy fractured in tension after solution treatment and quenching (no aging treatment); note the extensive grain distortion and the voids at and away from the fracture surface (V).

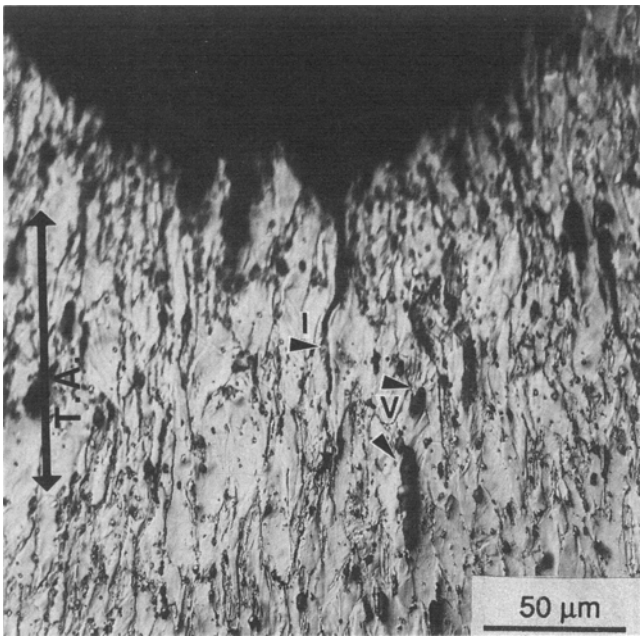

Fig. 15 Fracture surface profile of 430 alloy fractured in tension after aging at 475 °C for 500 hr; note the voids (V) and the high density of fine carbide precipitates.

smaller, uniform dimple structure of the 430 alloy is consistent with the reduced level of macroscopic ductility, as proposed by Williams *et al.*[22] The fracture behavior of the two alloys showed significant differences in response to aging at 475 °C. The 18SR alloy exhibited primarily brittle transgranular cleavage fracture with numerous intergranular cracks after aging 1000 hr at 475 °C, as shown in Fig. 9(a) through 9(c). Microvoids continued to dominate the fracture surfaces of the 430 alloy after a similar treatment (Fig. 10), with occasional intergranular cracks and some areas showing quasi-cleavage facets near the center of the fracture surface. The changing fracture patterns in both alloys and the greater susceptibility of the 18SR alloy to brittle transgranular cleavage fracture reflect the embrittling influence of increasing α' formation during continued aging. The greater severity of the α' reaction in the 18SR alloy is indicated by the steep decrease in ductility during aging and the increase in flow stress, which exceeds that of the 430 alloy within the initial 40 hr of aging, as shown in Fig. 4.

4.2 *475 °C Aging Reaction*

The apparent incubation period preceding the detection of the Cr-rich α' phase is consistent with the need for cufficient Cr diffusion to establish the solute rich zones. The rate of α' formation is expected to be much slower than the precipitation of carbides and nitrides in view of the relatively high mobility and low activation energy for the diffusion of carbon and nitrogen compared to chromium. The incubation period for the α' precipitation was less obvious for the 18SR alloy than for the 430 alloy. Detectable precipitation, as indicated by the increase in yield strength, occurred after 100 hr at 475 °C for the 430 alloy, compared to 25 hr for the 18SR alloy. After 1000 hr at 475 °C, the hardness and yield strength levels of the 18SR alloy increased to 304 DPH and 687 MPa, respectively, compared to 261 DPH and 597 MPa for the 430 alloy. The trends in the data at 400 °C are consistent, but the changes are less dramatic than those at 475 °C. The results point to the conclusion that 18SR is embrittled more rapidly and more severely than the 430 alloy. The higher hardness and yield stress values exhibited by the 18SR alloy could be accounted for by comparatively large coherency strains between α' and the ferrite matrix due to the presence of atomically large aluminum, silicon, and titanium solutes.

The dissolution of these elements in the α' phase is expected to increase the lattice parameter of the α' phase and intensify the coherency strains.[23,24] Alternatively, the higher hardness and strength of the 18SR alloy may reflect the strong solid solution-strengthening effect of aluminum in ferrite, although this was not apparent when comparing the two alloys in the solution-treated and quenched condition due to the strengthening effect of the dissolved interstitials in the 430 alloy. Grobner[25] indicated that the addition of about 2% Al should retard the onset of 475 °C embrittlement, but the present results indicate the opposite effect for the 18SR alloy. Spear[11] showed that 3 to 6% Al in iron-chromium-aluminum alloys inhibited, but did not prevent, the precipitation of α', because the reaction was detected within 50 hr at 475 °C. The presence of silicon and titanium is another factor contributing to the difference in behavior of the commercial 18SR alloy compared to the iron-chromium-aluminum ternary compositions.

The influence of increasing concentrations of aluminum on the strength and microstructural stability of iron-chromium alloys is demonstrated in Fig. 17, where the yield strength values for the 18SR and 430 alloys are compared with the data of Spear[11] for Fe-18Cr-3Al and Fe-18Cr-5Al alloys. Titanium and silicon are absent in the latter two alloys, therefore excluding any effects they might have with respect to the 18SR alloy. The ternary alloys containing no silicon or titanium also show

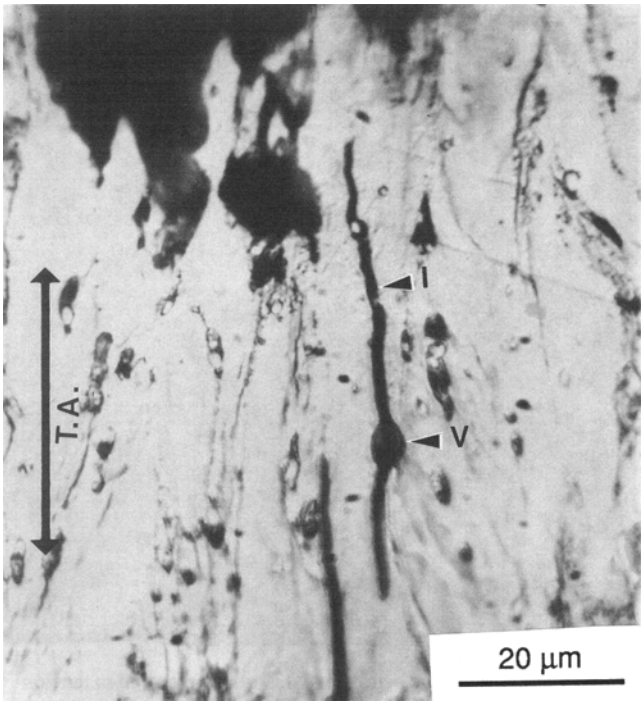

Fig. 16 Fracture surface profile of the 430 alloy fractured in tension after aging at 475 °C for 1000 hr; note the presence of intergranular cracking (I) and voids.

much more severe and rapid 475 °C embrittlement reaction than the 430 alloy, indicating that the addition of aluminum accelerates and intensifies rather than retards the embrittlement process.

4.3 *Intergranular Cracking*

The striking features of the microcracks observed in the 18SR and 430 alloys are their intergranular nature and their orientation generally parallel to the tensile axis. The susceptibility to microcracking increased with continued aging, with the most prominent effect being observed for aging at 475 °C. Intergranular cracking was not observed in the 430 alloy until after 500 hr of aging at 475 °C, whereas the 18SR alloy showed intergranular cracking after aging only 50 hr at 475 °C. Intergranular cracking parallel to the tensile axis has been reported previously in high chromium alloys, in which the 475 °C embrittlement reaction has not been detected.[26,27] In an Fe-21Cr-14Mn steel,[26] intergranular microcracks were attributed to the precipitation of $M_{23}C_6$ carbides at the grain boundaries. In a titanium-stabilized Fe-26Cr alloy, intergranular microcracking was observed in the unaged condition and attributed to titanium segregation at the boundaries, although there was no evidence of grain boundary precipitation.[27] However, the same alloy did not exhibit intergranular microcracking after aging at 475 °C. In the 18SR alloy of the present study, carbides and nitrides of titanium are present at the grain boundaries, as shown in Fig. 7(a). These boundary precipitates are effective initiating sites for voids that precede intergranular cracks, as shown in Fig. 11(b) and 12(b). Intergranular microcracking was not detected until the α′ precipitation reaction was initiated in the second stage of precipitation, thereby pointing to this reaction as a major catalyst for crack growth.

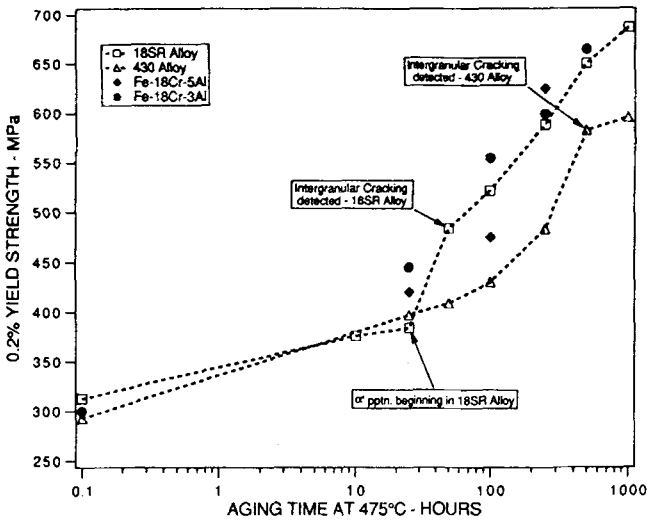

Fig. 17 Comparison of yield strength values as a function of aging time at 475 °C for the 18SR and 430 alloys with iron-chromium alloys containing 3 and 5% Al.

Several previous investigators[3,10,14,28-30] reported the formation of microcracks in conjunction with deformation twinning favored by α′ precipitation, but no evidence of twinning was observed in the present study. The absence of twinning in alloys containing only 18% Cr is consistent with the results of Imai *et al.*,[29] who showed that twins do not occur until the chromium content exceeds approximately 20%. The correlation of intergranular microcracking with the α′ reaction is substantiated further by the sharp decline in the value of the strain-hardening exponent during aging at 475 °C, as shown in Fig. 5. The detection of intergranular cracks corresponds to the aging times required to reduce the strain-hardening exponents from the initial values of approximately 0.2 to less than 0.12. This corresponded to approximately 50 hr at 475 °C, as illustrated in Fig. 11(a) and (b). The predominance of fine carbide precipitates in the 430 alloy accounts for the finer dimple structure on the fracture surfaces and indicates a larger number of localized plastic strain centers compared to the 18SR alloy. Such a condition should improve the capacity of the alloy to accommodate strain and limit strain concentration at the grain boundaries, as argued by Garrett and Knott[31] for aluminum alloys. This condition, together with the lower flow stress values for the 430 alloy, should reduce the susceptibility to intergranular cracking, even for similar levels of α′ formation, as observed in the present work.

Figures 9(b) and 10(a) show that most of the intergranular cracks in the 18SR alloy aged 1000 hr at 475 °C occur near the mid-thickness of the tensile specimen, with numerous voids or ductile dimples observed toward the outer surface. The fracture surface profiles showed necking prior to fracture, but the extent of necking was less for specimens subjected to increasing aging times. The grains, which were equiaxed prior to straining, were

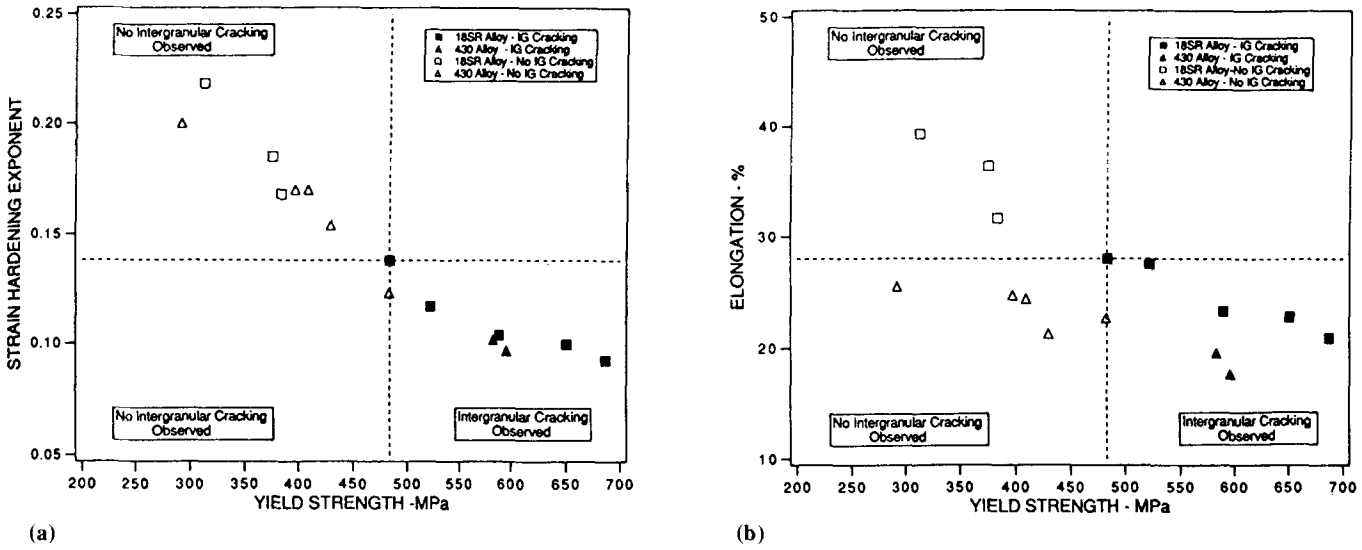

Fig. 18 Correlation between mechanical behavior and the occurrence of intergranular cracking. (**a**) Strain-hardening exponent as a function of 0.2% yield strength. (**b**) Elongation prior to fracture as a function of 0.2% yield strength.

elongated about 70% along the specimen axis in the necked region; the amount of elongation gradually decreased away from the central axis toward the outer surface. The preponderance of intergranular cracking toward the center axis of the tensile specimens is consistent with the development of a maximum transverse tensile stress component at the mid-section as necking proceeds.[32] The intergranular cracking parallel to the tensile axis is therefore attributed to the combined effects of void initiation at grain boundary precipitates, the reduced plasticity due to α' precipitation, and the triaxial stress components developed during necking.

4.4 *Intergranular Cracking and Mechanical Properties*

Figures 18(a) and (b), showing the strain-hardening exponent and the specimen elongation to fracture as functions of the yield stress for both alloys, provide a correlation between the mechanical properties and the occurrence of intergranular microcracking. The conditions corresponding to the initiation of microcracking are indicated by the horizontal and vertical dashed lines in both plots. The data points in the lower right quadrants correspond to the specimens exhibiting intergranular cracks. The plots suggest similar conditions apply for cracking in both the 18SR and 430 alloys; however, intergranular cracking is initiated in the 18SR alloy at lower yield stress levels than in the 430 alloy (483 versus 583 MPa). Furthermore, the 18SR alloy shows a higher elongation at a given yield strength than the 430 alloy, although the elongation plot (Fig. 18b) shows more scatter than the strain-hardening exponent plot.

The 430 alloy exhibited less elongation between the start of necking and the occurrence of failure than for the 18SR alloy; this can be attributed to the high propensity of voids nucleated by finely distributed chromium carbides and nitrides, especially along the grain boundaries. The 18SR alloy generally showed higher elongation than the 430 alloy for aging conditions producing similar 0.2% yield strength values; accordingly, the final neck thickness for the 18SR alloy is expected to be smaller than that for the 430 alloy. For example, the measured neck thickness at fracture for the 18SR alloy aged 50 hr at 475 °C was 275 μm, whereas that for the 430 alloy aged 250 hr at 475 °C, resulting in a similar yield value, was 310 μm. It was concluded that the greater localized reduction in thickness of the 18SR alloy accompanying necking makes it more susceptible than the 430 alloy to intergranular cracking in the axial direction due to the higher transverse stress component resulting from triaxiality at similar yield strength levels. Before longitudinal intergranular cracks are observed in the 430 alloy, longer aging times at 475 °C are required than for the 18SR alloy, to raise the flow stress so that the transverse stress component in the necked region is sufficient for intergranular crack initiation. The results therefore point to a combination of stress triaxiality in the necked region and sufficient α' precipitation as the key factors underlying intergranular crack growth.

5. Conclusions

Microstructural instabilities occur in Armco type 18SR and AISI 430 ferritic steels during aging at 400 to 550 °C; they are characterized by two reaction stages. The first stage is reflected by an increase in hardness and yield strength; it is followed by a period of aging, during which little or no property changes are detected. A second stage follows in which further increases in hardness and yield strength occur. Similar two-stage aging behavior is reflected by changes in the strain-hardening exponent and to a lesser degree, by changes in the elongation to fracture.

The property changes observed during the initial stage of aging are attributed to the precipitation of carbide and/or nitride particles. The 430 alloy exhibits more pronounced changes than the 18SR alloy during the first stage; this is due to the lower concentration of dissolved interstitials in the 18SR alloy at the solution temperature resulting from AlN and TiC formation.

The second reaction stage is identified with the 475 °C embrittlement reaction involving the precipitation of the chromium-rich α′ phase. This reaction occurs much faster during aging in the 18SR alloy and has more pronounced effects on the properties, probably due to the presence of aluminum, which is expected to increase the coherency strains associated with the α′ precipitation. Both alloys show an increasing susceptibility to intergranular cracking with aging time after the initiation of the second stage of aging when the flow stress is increasing and α′ precipitation is progressing. The observation of intergranular cracking during tension in the 18SR alloy after only 40 hr of aging compared to 500 hr for the 430 alloy attests to the important role of the α′ precipitation reaction in promoting this failure mode. The 18SR alloy also shows greater susceptibility to transgranular cleavage fracture and less ductile dimple fracture, also the result of an increased tendency for α′ precipitation. It was concluded that the fracture process in both alloys undergoes a transition with increasing aging times from ductile dimple to intergranular fracture to a mix of intergranular and transgranular cleavage. The occurrence of intergranular fracture is favored by the combined effects of reduced plasticity in regions adjacent to grain boundaries resulting from α′ precipitation and the transverse stress components due to triaxiality after the onset of necking prior to fracture.

Acknowledgments

The authors thank Dr. P.J. Moroz of the Armco Steel Corp. for supplying materials for this study. Thanks are also due to Dr. W.S. Spear for helpful discussions and assistance during the progress of the work.

References

1. R.M. Fisher, E.J. Dulis, and K.G. Carroll, *Trans. AIME, 197*, 690-695 (1953).
2. R.O. Williams and H.W. Paxton, *J. Iron Steel Inst., London, 185*, 358-374 (1957).
3. M.J. Blackburn and J. Nutting, *J. Iron Steel Inst., London, 202*, 610-613 (1964).
4. O. Kubaschewski and T.G. Chart, *J. Inst. Metals, 93*, 329-338 (1964-65).
5. M.J. Marcinkowski, R.M. Fisher, and A. Szirmae, *Trans. AIME, 230*, 676-689 (1964).
6. R. Lagneberg, *Trans. ASM, 60*, 67-78 (1967).
7. T. De Nye and P.M. Gehlen, *Met. Trans., 2*, 1423-1428 (1971).
8. D. Chandra and L.H. Schwartz, *Met. Trans., 2*, 511-519 (1971).
9. W.O. Binder and H.R. Spendelow, Jr., *Trans. ASM, 43*, 759-772 (1951).
10. A. Plumtree and R. Gullberg, *Met. Trans., 7A*, 1451-1458 (1976).
11. W.S. Spear, Ph.D. dissertation, University of Washington (1987).
12. R.A. Perkins, "Materials for Coal Conversion and Utilization," Energy Research and Development Association, Conference, Gaithersburg, Maryland, 77-1025, 11-26, Oct (1977).
13. H. Ishii and Y. Hujimura, *J. Jpn. Inst. Metals, 39*, 311-317 (1975).
14. H. Thielsch, *Welding J., 34*, 225 (1955).
15. J.J. Demo, *Corrosion, 27*(12), 531 (1971).
16. K. Woltron, *Berg Huttenmaennische Monatsch., 116*, 429 (1972).
17. R.N. Wright, "Toughness of Ferritic Stainless Steels," ASTM STP 706, R.A. Lula, Ed., ASTM, Philadelphia, 2-33 (1980).
18. T.J. Nichol, A. Datta, and G. Aggen, *Met. Trans., 11A*, 573-585 (1980).
19. G. Aggen, H.E. Edeverell, and T.J. Nichol, "*Micon 78*," ASTM STP 672, 334-369 (1979).
20. A.W. Thompson and J.C. Williams, *Fracture 1977*, Vol. 2A, ICF4, Waterloo, Canada, 343-348 (1974).
21. I.M. Wolff and A. Ball, *Acta Metall. Mater., 39*(11), 2759-2770 (1991).
22. J.C. Williams, R.R. Boyer, and M.J. Blackburn, "Electron Microfractography," ASTM STP 453, ASTM, Philadelphia, 215-235 (1968).
23. T.J. Nichol, *Met. Trans., 8A*, 229-237 (1977).
24. P. Koutanieni, V. Heikkeinen, and A. Saarinen, *Metal Sci., 8*, 94-96 (1974).
25. B.J. Grobner, Report No. RP-33-71-02, Climax Molybdenum Co., Jan (1974).
26. T. Yasunaka, *Trans. Nat. Res. Inst. Met., 22*(3), 10-18 (1980).
27. J.F. Grubb, R.N. Wright, and P. Farrar, Jr., "Toughness of Ferritic Stainless Steels," ASTM STP 706, R.A. Lula, Ed., ASTM, Philadelphia, 56-76 (1980).
28. A.I. Kondyr, A.N. Tkach, V.I. Atashkin, and M. Zamora, *Fiz. Khim. Mekh. Mater., 10*, 24-28 (1974).
29. Y. Imai, K. Nishino, and Y. Nakagawa, *J. Jpn. Inst. Metals, 29*(4), 346-350 (1965).
30. T. Yasunaka and M. Kanao, *Transactions of the Iron and Steel Institute of Japan, 19*, 69-75 (1979).
31. G.G. Garrett and J.F. Knott, *Met. Trans., 9A*, 1187-1201 (1978).
32. A. Nadai, *Theory of Flow and Fracture of Solids*, McGraw-Hill, New York (1950).